

Cite this: *Chem. Sci.*, 2020, **11**, 5902

All publication charges for this article have been paid for by the Royal Society of Chemistry

# Spontaneous mirror symmetry breaking in benzil-based soft crystalline, cubic liquid crystalline and isotropic liquid phases†

Tino Reppe,<sup>a</sup> Silvio Poppe,<sup>a</sup> Xiaoqian Cai,<sup>b</sup> Yu Cao,<sup>b</sup> Feng Liu<sup>id</sup>\*<sup>b</sup> and Carsten Tschierske<sup>id</sup>\*<sup>a</sup>

Benzil (diphenylethane-1,2-dione), which is a long known example for an achiral molecule crystallizing in a chiral space group, can also show mirror symmetry breaking in the fluid state if it is suitably functionalized. For some of the new benzil derivatives even three different subsequent mirror symmetry broken soft matter states with a chiral conglomerate structure can be observed. One is an isotropic liquid, the second one a cubic liquid crystal with a complex network structure and the third is a soft crystalline solid. Chirality develops by helical self-assembly combined with dynamic network formation, thus allowing macroscopic chirality synchronization. These achiral molecules, combining a transiently chiral bent core with multiple alkyl chains, provide a unique link between the mirror symmetry breaking phenomena observed for polycatenar and bent-core mesogens. The homogeneously chiral networks are of interest for application as chiral materials, and as templates for chiral recognition, separation and enantioselective catalysis.

Received 8th March 2020

Accepted 29th April 2020

DOI: 10.1039/d0sc01396j

rsc.li/chemical-science

Mirror symmetry breaking and development of uniform chirality is considered essential for the development of life. Understanding and controlling the formation of chirality is crucial across different disciplines. In biosystems the chirality of nucleic acids, sugars and amino acids enables the formation of the helical nanostructures of DNA and proteins.<sup>1</sup> Enantioselective synthesis, catalysis and autocatalysis<sup>2</sup> were successfully developed during recent decades for the synthesis of enantiopure molecules from achiral precursors. This requires expensive chiral reagents or catalysts, synthesized in multistep processes from the chiral pool of nature. However, there is a more economic approach to homochirality, because it can also emerge spontaneously as a result of physical processes such as crystallization,<sup>3</sup> as for example shown for the Viedma ripening,<sup>4</sup> where rapidly enantiomerizing racemic mixtures of chiral molecules, or even achiral molecules crystallizing in a chiral space group spontaneously form uniform chiral crystals with optical activity (OA). The combination of generation of chiral centers with deracemization by dynamic crystallization provides a new absolute asymmetric synthesis methodology.<sup>5</sup>

Likewise, spontaneous chirality can also emerge during the formation of liquid crystalline (LC) phases and even in liquids due to a dynamic process of chirality synchronization,<sup>6</sup> which is the subject of this contribution.

One of the most prominent examples of achiral molecules crystallizing in a chiral space group is benzil (**1**, Fig. 1a), whose OA has been more closely studied than for any other organic crystal.<sup>7,8</sup> In the chiral crystal structure the molecules assume a helical conformation with a torsion angle of the O=C–C=O bond of about  $\alpha = 110^\circ$ .<sup>7</sup> This twisted (skewed) cisoid conformation is also found as a preferred conformation in the gas phase<sup>9</sup> and in solution.<sup>10</sup> However, the energy barrier for the rotation around the O=C–C=O bond is relatively low and in solution or in the melted state it leads to optical inactivity. Thus benzil is a typical transiently chiral molecule capable of mirror symmetry breaking in the crystalline state by Viedma ripening.<sup>11</sup>

Recently, we have observed emergence of OA in bicontinuous cubic (Cub<sub>bi</sub>) LC phases<sup>12</sup> (Fig. 1d) and even in isotropic liquids (Iso<sub>1</sub><sup>[\*]</sup>) by formation of conglomerates of chiral domains.<sup>13</sup> This OA is related to the helical nano-scale organization of the molecules in these Cub<sub>bi</sub> and Iso<sub>1</sub><sup>[\*]</sup> phases.<sup>6</sup> The question arises whether the transient chirality of the benzil unit can support the development of this spontaneous dissymmetry. Moreover, the twisted conformation leads to a non-linear bent shape of the aromatic core, providing some similarity to bent-core molecules, which are also known for their capability of showing mirror symmetry breaking.<sup>14–16</sup> In this case besides helix formation the reduction of the phase symmetry to C<sub>2v</sub>, due

<sup>a</sup>Institute of Chemistry, Martin Luther University Halle-Wittenberg, Kurt-Mothes-Straße 2, 06120 Halle, Germany. E-mail: carsten.tschierske@chemie.uni-halle.de

<sup>b</sup>State Key Laboratory for Mechanical Behaviour of Materials, Shaanxi International Research Center for Soft Matter, Xi'an Jiaotong University, Xi'an 710049, P. R. China. E-mail: feng.liu@xjtu.edu.cn

† Electronic supplementary information (ESI) available. See DOI: 10.1039/d0sc01396j

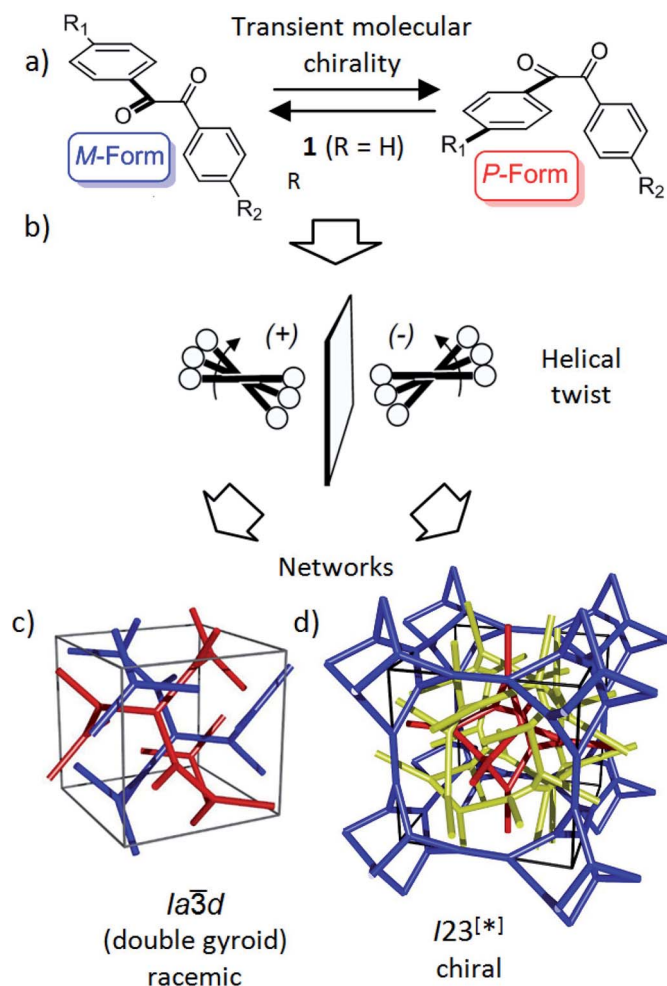


Fig. 1 Schematics showing (a) the transient chirality of benzil derived molecules; and (b) the development of the helical twist by clashing of the bulky end groups attached to the cores and (c and d) the network structure of the Cub<sub>bi</sub> phases under discussion.<sup>25</sup> The benzil based polyaromatic cores form the helical networks which are embedded in the continuum filled by the terminal chains. (c and d) were reproduced from ref. 25 by permission of The Royal Society of Chemistry.

to the organization of the tilted molecules with their bent direction parallel to the layer planes (see Fig. S16<sup>†</sup>), contributes to symmetry breaking.<sup>14</sup>

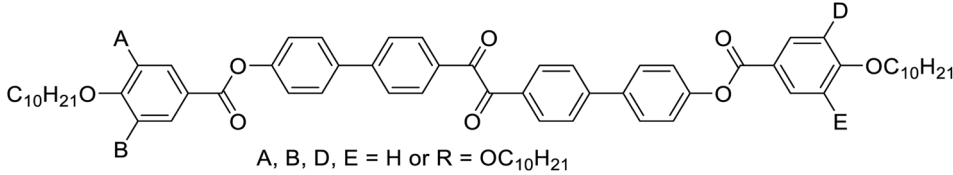
Besides the well-known case of lyotropic LCs,<sup>17</sup> Cub<sub>bi</sub> phases are also known to be formed in solvent-free (thermotropic) systems by rod-like polyaromatic molecules with two<sup>18,19</sup> or multiple alkyl end-chains (polycatenar compounds),<sup>20</sup> branched chains (swallow tailed compounds)<sup>21</sup> or other bulky end groups.<sup>22</sup> In these Cub<sub>bi</sub> phases the rods form networks and the alkyl chains fill the space between them (Fig. 1c and d). Within the networks the orientation of the rods is perpendicular or slightly tilted with respect to the local network direction and the mismatch of the cross sectional areas of these cores with the cross sectional area of the terminally attached chains leads to the curvature of the aggregates, and simultaneously, to a helical twist along the networks (Fig. 1b).<sup>6,12a</sup> There are two major types of such thermotropic Cub<sub>bi</sub> phases, the double gyroid phase

(space group  $Ia\bar{3}d$ ) and the triple network phase designated as  $Im\bar{3}m$  (Fig. 1c and d).<sup>18,23,24</sup> The  $Ia\bar{3}d$  phase involves two helical networks with opposite handedness (red, blue in Fig. 1c) and therefore it is achiral.<sup>12a</sup> However, in the  $Im\bar{3}m$  phase this degeneracy is broken by the presence of three networks<sup>24</sup> and the synchronization of the helix sense between them.<sup>12a</sup> The chiral space group with the highest symmetry, derived from the achiral  $Im\bar{3}m$  space group would be  $I432$ ,<sup>12</sup> but the actual space group was recently identified as  $I23$ .<sup>25</sup> In this new structural model of the “ $Im\bar{3}m$ ” type Cub<sub>bi</sub> phase there are three networks with all junctions being threefold, but with distances and twist angles between the junctions being slightly different from those in the  $Ia\bar{3}d$  phase (Fig. 1d).

Herein we report the first mirror symmetry broken LC phases formed by a series of suitably designed multi-chain benzil derivatives (Tables 1 and 2). The decyloxy substituted compounds with a different number of chains are labelled as 2–6 according to their order in Table 1. Compounds 3 have three decyloxy chains at one end and either no chain (compound 3/H) or a single *n*-alkyloxy chain with a variable length at the other end (compounds 3/*n*); here the number *n* after the slash indicates the length of this chain (Table 2). The respective compounds were synthesized as described in Scheme S1<sup>†</sup> and the experimental procedures are given in the ESI.<sup>†</sup> Analysis of their self-assembly was performed by polarizing optical microscopy (POM), differential scanning calorimetry (DSC) and X-ray diffraction (XRD). As is obvious from Table 1, with the growing number of *n*-decyl chains a transition from lamellar (SmC, 2) via two different types of Cub<sub>bi</sub> phases ( $Ia\bar{3}d$ ,  $I23^{[*]}$ , 3/10, 4) to hexagonal columnar phases (Col<sub>hex</sub>, 4, 5) is observed. Only the hexaalkyl substituted compound 6 does not show any LC phase. The SmC and Col<sub>hex</sub> phases were indicated by their typical birefringent optical textures observed between crossed polarizers (Fig. 2e, h and S2–S5<sup>†</sup>) and were confirmed by XRD for compounds 2 and 5 (Table S6<sup>†</sup>). The transition from the isotropic liquid state (Iso) to the Cub<sub>bi</sub> phases was indicated by a small exotherm in the DSC scans, accompanied by an increase in the viscosity while the phase remained optically isotropic. The cubic phase types are distinguished by optical investigation between polarizers, rotated by a small angle ( $\sim 5^\circ$ ) out of the  $90^\circ$  crossed orientation, where only the  $I23$  phase shows a conglomerate of optically active (dark and bright) domains ( $I23^{[*]}$  phase), whereas  $Ia\bar{3}d$  is optically inactive (Fig. 2f and g).<sup>12</sup> Interestingly, the Cub<sub>bi</sub> phase type depends on the chain distribution and the chain length (Tables 1 and 2); for the symmetric compound 4 the achiral  $Ia\bar{3}d$  phase occurs as a monotropic (metastable) phase below Col<sub>hex</sub>, whereas the non-symmetric compound 3/10 has exclusively a broad range of the mirror symmetry broken  $I23^{[*]}$  phase. To the best of our knowledge, these are the first benzil derivatives forming cubic LC phases, whereas a few benzil based compounds involving amide groups were found to form exclusively columnar LC phases.<sup>26</sup>

Here we focus on the homologous series of the non-symmetric tetracatenars 3/*n* where only 3/H and 3/1 are non-mesomorphic and all the following homologues form Cub<sub>bi</sub> phases (Table 2). In this series the Cub<sub>bi</sub> phase type changes



Table 1 Phase transitions of compounds 2–6 on heating<sup>a</sup>


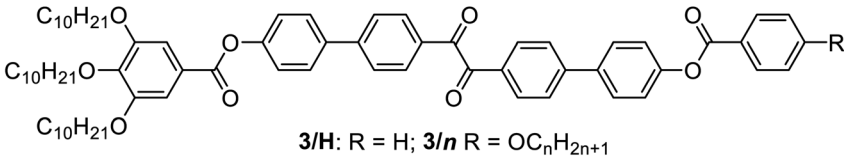
A, B, D, E = H or R = OC<sub>10</sub>H<sub>21</sub>

Compd.	A	B	D	E	<i>T</i> /°C [ $\Delta H$ kJ mol <sup>-1</sup> ]
2	H	H	H	H	Cr 149 [27.0] SmC <sup>b</sup> 243 [12.0] Iso
3/10	R	R	H	H	Cr 97 [63.2] (Cr <sub>Iso</sub> <sup>[*]</sup> 90 [17.6]) <b>Cub<sub>bi</sub>/I23<sup>[*]</sup></b> 131 [2.2] Iso <sub>1</sub> 138 [5.7] Iso
4	R	H	R	H	Cr 151 [69.5] (Cub <sub>bi</sub> /Ia3d 141 Col <sub>hex</sub> 143 [12.4] <sup>c</sup> ) Iso
5	R	R	R	H	Cr 92 [14.2] Col <sub>hex</sub> <sup>d</sup> 105 [7.1] Iso
6	R	R	R	R	Cr 84 [33.2] Iso

<sup>a</sup> DSC peak temperatures at 10 K min<sup>-1</sup>; values in round parantheses indicate monotropic phases, only observed on cooling; abbreviations: Cr = crystalline solid, SmC = tilted lamellar phase, Cub<sub>bi</sub>/Ia3d = achiral Cub<sub>bi</sub> phase with the Ia3d space group, Cub<sub>bi</sub>/I23<sup>[\*]</sup> = mirror symmetry broken Cub<sub>bi</sub> phase with the I23 space group; Iso = achiral isotropic liquid; Iso<sub>1</sub><sup>[\*]</sup> = mirror symmetry broken Iso phase; for DSC traces, see Fig. S1, and for textures, see Fig. S2–S5. <sup>b</sup> *d* = 3.66 nm. <sup>c</sup> Enthalpies of both transitions. <sup>d</sup> *a*<sub>hex</sub> = 4.39 nm.

from Ia3d (*n* = 2) via I23<sup>[\*]</sup> (*n* = 4–10) to Ia3d again (*n* = 12–16), upon chain elongation. The high resolution diffraction patterns of the I23<sup>[\*]</sup> phase of 3/4 and the Ia3d phase of 3/16, recorded

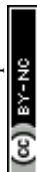
with a synchrotron source, are shown as representative examples in Fig. 2a and b. Besides the diffuse wide angle scattering (Fig. S7b and c†), there are several sharp small angle scatterings,

Table 2 Phase transitions, lattice parameters (*a*<sub>cub</sub>), number of molecules in the neighbouring rafts (*n*<sub>raft</sub>) and twist angles between the rafts ( $\Phi$ /°) in the Cub<sub>bi</sub> phases of compounds 3/H and 3/*n*<sup>a</sup>


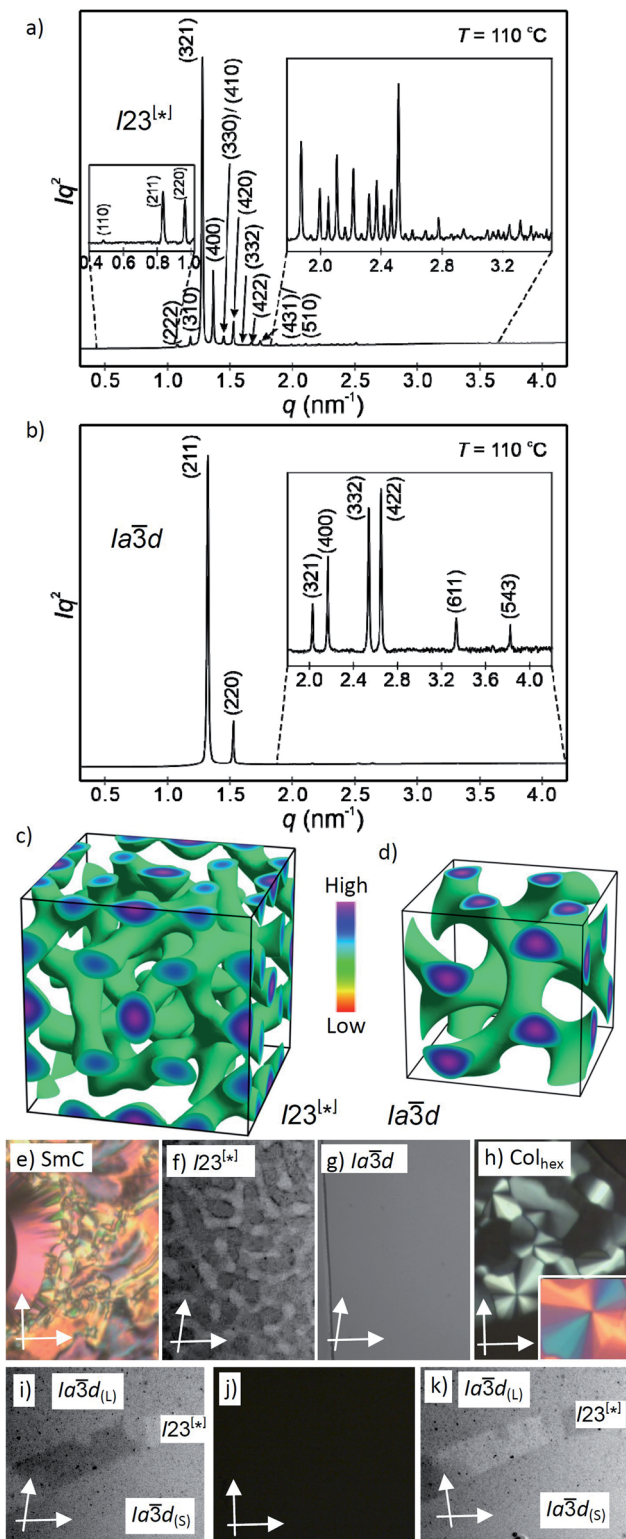
3/H: R = H; 3/*n* R = OC<sub>n</sub>H<sub>2n+1</sub>

3/ <i>n</i>	<i>T</i> /°C [ $\Delta H$ kJ mol <sup>-1</sup> ]	<i>a</i> <sub>cub</sub> /nm	<i>n</i> <sub>raft</sub>	$\Phi$ /°	<i>L</i> <sub>mol</sub> /nm
3/H	H: Cr 126 [52.2] Iso C: Iso 110 [27.3] Cr	—	—	—	4.2
3/1	H: Cr 127 [36.3] Iso C: Iso 115 [36.4] Cr	—	—	—	4.3
3/2	H: Cr 120 [37.9] Ia3d <sub>(L)</sub> 127 [1.8] Iso <sub>1</sub> 135 [2.8] Iso C: Iso 133 [2.7] Iso <sub>1</sub> 121 [0.2] <b>Iso<sub>1</sub><sup>[*]</sup></b> 110 [0.3] Ia3d <sub>(L)</sub> 105 [31.3] Cr	12.9	5.0	6.9	4.4
3/4	H: Cr 128 [53.5] Iso C: Iso 128 [4.5] Iso <sub>1</sub> 122 [0.4] <b>Iso<sub>1</sub><sup>[*]</sup></b> 116 [0.7] <b>I23<sup>[*]</sup></b> 73 [21.2] Cr	18.4	4.0	7.6	4.6
3/6	H: Cr 118 [64.6] (Cr <sub>Iso</sub> <sup>[*]</sup> 82 [17.3]) <b>I23<sup>[*]</sup></b> 126 [2.2] Iso <sub>1</sub> 134 [5.7] Iso C: Iso 130 [7.1] Iso <sub>1</sub> 123 [0.5] <b>Iso<sub>1</sub><sup>[*]</sup></b> 118 [1.1] <b>I23<sup>[*]</sup></b> 61 [15.3] Cr <sub>Iso</sub> <sup>[*]</sup>	18.1	3.8	7.7	4.8
3/10	H: Cr 97 [63.2] (Cr <sub>Iso</sub> <sup>[*]</sup> 90 [17.6]) <b>I23<sup>[*]</sup></b> 131 [2.2] Iso <sub>1</sub> 138 [5.7] Iso C: Iso 135 [5.9] Iso <sub>1</sub> 127 [0.3] <b>Iso<sub>1</sub><sup>[*]</sup></b> 122 [0.9] <b>I23<sup>[*]</sup></b> 66 [17.8] Cr <sub>Iso</sub> <sup>[*]</sup>	18.4	3.7	7.6	5.2
3/12	H: Cr 114 [47.0] Ia3d <sub>(S)</sub> 135 [3.4] Iso <sub>1</sub> 139 [6.2] Iso C: Iso 137 [8.9] Iso <sub>1</sub> 128 [0.3] <b>Iso<sub>1</sub><sup>[*]</sup></b> 122 [0.7] Ia3d <sub>(S)</sub> 48 [17.9] Cr <sub>Iso</sub> < 20 Cr	11.4	3.3	7.9	5.4
3/14	H: Cr 108 [44.1] Ia3d <sub>(S)</sub> 135 [2.7] Iso <sub>1</sub> 138 [7.2] Iso C: Iso 136 [9.2] Iso <sub>1</sub> 129 [1.4] Col <sub>hex</sub> 125 [0.5] Ia3d <sub>(S)</sub> 42 [16.9] Cr <sub>Iso</sub> < 20 Cr	11.3	3.2	7.8	5.6
3/16	H: Cr 80 [36.4] Ia3d <sub>(S)</sub> 133 [3.1] Iso <sub>1</sub> 139 [6.1] Iso C: Iso 136 [6.0] Iso <sub>1</sub> 130 [2.3] Col <sub>hex</sub> 121 [0.5] Ia3d <sub>(S)</sub> 45 [25.0] Cr	11.5	3.2	7.8	5.8

<sup>a</sup> DSC peak temperatures on heating/cooling (H/C) at 10 K min<sup>-1</sup>; *n*<sub>raft</sub> = *n*<sub>cell</sub>/(*L*<sub>net</sub>/0.45) with *L*<sub>net</sub> = 20.68*a*<sub>I23</sub>; and *L*<sub>net</sub> = 8.485*a*<sub>Ia3d</sub>;  $\Phi$ (Ia3d) = 70.5°/[0.354*a*<sub>cub</sub>/0.45 nm];  $\Phi$ (I23) = 90°/[0.290*a*<sub>cub</sub>/0.45 nm];<sup>25</sup> *L*<sub>mol</sub> = maximum molecular length as determined with space filling models assuming a molecular bend of 110° and all-*trans* alkyl chains, see Fig. S15; abbreviations: Iso<sub>1</sub> = achiral cybotactic isotropic liquid (see Fig. 3d), Cr = birefringent crystalline solid; Cr<sub>Iso</sub> = optically isotropic crystalline mesophase; Cr<sub>Iso</sub><sup>[\*]</sup> = mirror symmetry broken Cr<sub>Iso</sub> forming a conglomerate of chiral domains; Ia3d<sub>(S)</sub> = short pitch Ia3d phase with a smaller number of molecules in the unit cell/rafts and a larger twist angle  $\Phi$  than in Ia3d<sub>(L)</sub> = long pitch Ia3d phase with a larger number of molecules in the unit cell/rafts and a smaller twist angle  $\Phi$ ; for other abbreviations, see Table 1; chiral phases are shown in bold; because the transitions Iso–Iso<sub>1</sub> are very broad (see Table S1) it is difficult to determine precise enthalpy values; for DSC traces, see Fig. S1 and for XRD data, see Tables S1–S7 and Fig. S7 and S10–S14.







**Fig. 2** (a and b) SAXS diffractograms of the  $I23^{[*]}$  (3/4) and the  $la\bar{3}d_{(S)}$  (3/16) phases (for the synchrotron source and for numerical data, see Tables S4 and S5;† the full indexations of the  $I23^{[*]}$  phase and the WAXS scans are shown in Fig. S7†); (c and d) reconstructed electron density maps of the  $I23^{[*]}$  and  $la\bar{3}d_{(S)}$  phase; the aromatic cores are located in the networks formed by the green iso-surfaces, the space between is filled by the alkyl chains; for more details, see the ESI, and Fig. S8† for the individual networks; (e–h) the textures of the (e) SmC phase of 3/10 at  $230^\circ\text{C}$ ; (f) the  $\text{Cub}_{bi}/I23^{[*]}$  phase of 3/10 at  $121^\circ\text{C}$  and

the strongest being indexed either to (211) and (220) of the  $Ia\bar{3}d$  lattice or (321), (400) and (420) reflections of the  $I23^{[*]}$  lattice. The electron density maps (Fig. 2c, d and S9†) reconstructed from these patterns are in agreement with the proposed phase structures shown schematically in Fig. 1c and d. The method of selecting the correct phase combination is described in previous work.<sup>12,25,27</sup> The cubic lattice parameter is around 11–13 nm for  $Ia\bar{3}d$  and 18 nm for  $I23^{[*]}$ , in line with a double- and triple-network structure, respectively. Remarkably, the  $Ia\bar{3}d$  lattice is the largest for the smallest molecule 3/2 ( $L_{\text{mol}} = 4.4$  nm;  $a_{\text{cub}} = 12.9$  nm) and becomes smaller for the  $Ia\bar{3}d$  phases of the larger compounds 3/12–3/16 with much longer chains ( $L_{\text{mol}} = 5.8$ – $6.3$  nm;  $a_{\text{cub}} = 11.3$ – $11.5$  nm).<sup>28</sup> In line with this, in the  $Ia\bar{3}d$  phase of 3/2 about 5 molecules are arranged side-by-side in the cross section of the networks, whereas for 3/12–3/16 there are only 3.2 molecules (Tables 2 and S7†). The twist between the molecules in the adjacent rafts with a height of 0.45 nm ( $\Phi$ ) can be calculated as  $\sim 7^\circ$  in the long pitch  $Ia\bar{3}d_{(L)}$  phase of 3/2 and  $\sim 8^\circ$  for the short pitch  $Ia\bar{3}d_{(S)}$  phase of compounds 3/12–3/16 (Table 2). The intermediate homologues 3/4–3/10 escape from forming the  $Ia\bar{3}d$  phase by assuming the triple network  $I23^{[*]}$  structure instead. The twist in this network is almost constant  $7.6$ – $7.7^\circ$  and between the angles in the  $Ia\bar{3}d_{(L)}$  and  $Ia\bar{3}d_{(S)}$  phases. The  $I23^{[*]}$  phase obviously allows for these twist angles a better fit of the helical pitch length with junction distances and inter-junction twist angles than in the competing  $Ia\bar{3}d$  lattices.<sup>12a,25</sup> This phase sequence was also reported for the  $\text{Cub}_{bi}$  phases of other rod-like molecules<sup>18a,19,29</sup> and it is observed in the contact regions between the achiral  $Ia\bar{3}d_{(L)}$  and  $Ia\bar{3}d_{(S)}$  phases of 3/2 and 3/12–3/16, respectively, where a concentration gradient develops, and in a certain concentration range the chiral conglomerate of the  $I23^{[*]}$  phase is induced (Fig. 2i–k).<sup>29,30</sup>

In addition to the cubic phases, for compounds 3/2–3/12 a mirror symmetry broken isotropic liquid ( $\text{Iso}_1^{[*]}$  phase) occurs as a metastable (monotropic) phase on cooling the achiral  $\text{Iso}$  phase and replaces a part of the  $\text{Cub}_{bi}$  phase range (Table 2). The  $\text{Iso}_1^{[*]}$  phase disappears at the transition from  $n = 12$  to 14 right after the transition from  $I23^{[*]}$  to  $Ia\bar{3}d_{(S)}$  occurring from  $n = 10$  to 12. Hence, it can be concluded that the local structure in the  $\text{Iso}_1^{[*]}$  phase is likely to be related to that of the chiral  $I23^{[*]}$  triple network (Fig. 1d). Remarkably, for 3/2–3/12 the transition  $\text{Iso}$ – $\text{Iso}_1^{[*]}$  takes place in two separate steps, as indicated by the DSC trace of 3/12 (Fig. 3a). A very broad feature within the isotropic liquid range (with a maximum around  $137^\circ\text{C}$  on cooling) indicates the transition from an ordinary

(g)  $\text{Cub}_{bi}/Ia\bar{3}d_{(S)}$  phase of 3/12 at  $120^\circ\text{C}$ , as observed between slightly uncrossed polarizers; (h)  $\text{Col}_{hex}$  phase of 3/10 at  $141^\circ\text{C}$ ; the inset shows the texture with an additional  $\lambda$ -plate, indicating that the phase is optically negative, i.e. the orientation of the aromatic cores is perpendicular or only slightly tilted to the column long axis; (i–k) show the induced chiral  $I23^{[*]}$  phase in the contact region between the achiral  $Ia\bar{3}d_{(L)}$  phase of 3/2 (top) and the  $Ia\bar{3}d_{(S)}$  phase of 3/16 (bottom); the orientation of the polarizers is shown by white arrows; the width of the POM images in (e–k) is  $200\ \mu\text{m}$ , and in (f), (i) and (k) the contrast is enhanced; for additional textures, see also Fig. S2–S6.†

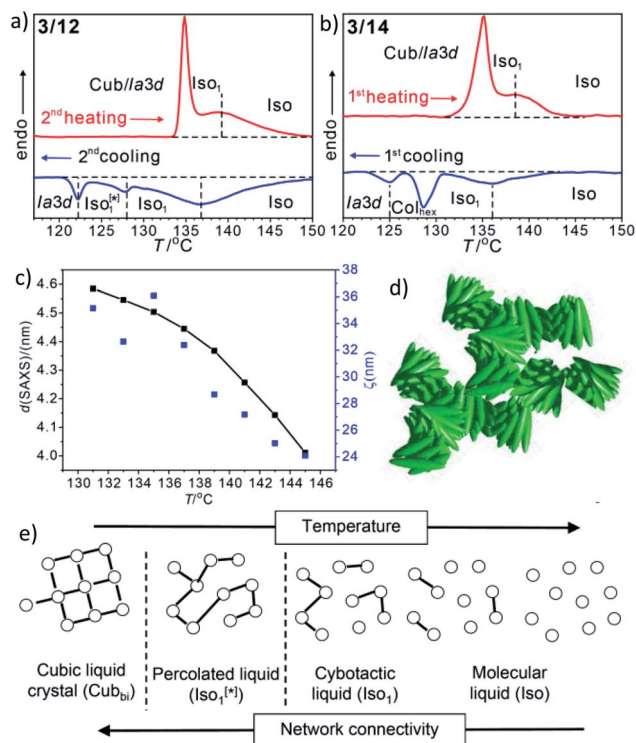


Fig. 3 (a and b) sections of the DSC traces ( $10 \text{ K min}^{-1}$ ) of compounds 3/12 and 3/14 (see Fig. S1† for complete traces); (c) plot of the  $d$ -values (black) and the correlation length ( $\zeta$ , blue) of the small angle scattering of 3/12 in the isotropic liquid phases (see also Fig. S10 and S11†); (d) sketch of the fused helical clusters in the  $\text{Iso}_1^{[*]}$  phase; (e) schematic sketch showing the transition from Iso via a cybotactic and a percolated liquid to  $\text{Cub}_{\text{bi}}$  by increasing the transient network connectivity; the dots represent locally ordered clusters, the lines indicate the connections between them, and the vertical dotted lines indicate phase transitions.

isotropic liquid (Iso) to a kind of cybotactic isotropic liquid with a fluctuating local network structure ( $\text{Iso}_1$ ),<sup>31</sup> which is still achiral (Tables 2 and S1†). With further decrease in the temperature the number of linkages between the clusters increases. Mirror symmetry breaking sets in at the next much sharper transition at  $128^\circ\text{C}$  which we attribute to the transition from the cybotactic to a percolated liquid, after crossing a certain critical density of connectivity between the cybotactic clusters,<sup>6a,32</sup> thus leading to a long range transmission of the helical twist, and hence, chirality ( $\text{Iso}_1^{[*]}$ ). In the  $\text{Iso}_1^{[*]}$  range the connections are transient and at the next transition at  $122^\circ\text{C}$  they become permanent with formation of the  $Ia\bar{3}d$  phase (or  $I23^{[*]}$  for the shorter homologues, Fig. 3e). In the temperature range of the isotropic liquid phases there is an almost continuous increase in the line width of the small angle XRD scattering (Fig. 3c) and there is also no obvious discontinuity in the viscosity, as indicated by optical microscopy, where all three isotropic liquid phases flow under the influence of gravity. Only at the transition to the cubic phase the material suddenly becomes viscoelastic. The enthalpy of the  $\text{Iso}-\text{Iso}_1$  transition increases with the growing chain length with a distinct jump from  $n = 4$  to 6 (Table 2), in line with improved rod-chain segregation, supporting the cluster formation.

For the longer homologues 3/14 and 3/16 the  $\text{Iso}_1^{[*]}$  phase is replaced by a  $\text{Col}_{\text{hex}}$  phase (Fig. 3b). The growing chain length obviously disfavours the branching, thus leading to predominately linear aggregates which do not form networks, but assume long range order and transform to the achiral  $\text{Col}_{\text{hex}}$  phase.

Another interesting feature of compounds 3/6–3/10 is that on further cooling from the  $\text{Cub}_{\text{bi}}/I23^{[*]}$  phase a transition to an optically isotropic crystalline mesophase is observed, in which, the conglomerate texture is retained ( $\text{Cr}_{\text{Iso}}^{[*]}$  phase, see Fig. 4c–f). Because this transition is associated with a change in the XRD pattern and a sharp transition with a significant transition enthalpy of  $17\text{--}18 \text{ kJ mol}^{-1}$  (Table 2 and Fig. 4g), it cannot be a glass transition. The XRD pattern of the  $\text{Cr}_{\text{Iso}}^{[*]}$  phase is characterized by a relatively broad small angle scattering, with a maximum at  $d = 5.38 \text{ nm}$  for 3/6 (Fig. 4h) and  $5.45 \text{ nm}$  for 3/10, approximately corresponding to the lengths of the respective intercalated anti-parallel molecular pairs ( $5.5 \text{ nm}$ , see Fig. S15†). In the wide angle range, there are three broad scatterings with very low intensity (Fig. 4i, S12 and S13†), which can tentatively be attributed to the mean alkyl chain distance ( $0.44 \text{ nm}$ ) and the edge-to-edge and face-to-face packing distances of the aromatics ( $0.56/0.37 \text{ nm}$ ). This diffraction pattern is similar to those typically recorded for the symmetry broken soft crystalline mesophases of bent-core mesogens, helical nanofilaments (HNFs),<sup>16,33a</sup> helical nano-crystallites (HNCs)<sup>34</sup> and related helical phases,<sup>35</sup> which in some respect can be considered as solvent free gels.<sup>16,36,37</sup> A transition from the LC  $\text{Cub}_{\text{bi}}$  phase to a soft crystalline network structure, where the polyaromatic rods and parts of the aliphatic chains assume a crystalline packing, appears likely. Similar to the bent-core mesogens, the directed packing of the twisted and bent 4,4'-diphenylbenzil units (Fig. S15†) is likely to contribute to the development of the helical packing modes in the liquid, LC and especially in the soft crystalline mesophases of compounds 3/ $n$ . For compounds 3/12 and 3/14, forming the achiral  $Ia\bar{3}d_{\text{(s)}}$  cubic phase instead of  $I23^{[*]}$ , the isotropic crystalline phase appears to be achiral ( $\text{Cr}_{\text{Iso}}$ , see Fig. S6†), though the XRD pattern (Fig. S14†) is almost the same as for 3/6 and 3/10. Whether this phase is intrinsically achiral, or the symmetry breaking at the transition from the achiral  $Ia\bar{3}d_{\text{(s)}}$  to a  $\text{Cr}_{\text{Iso}}^{[*]}$  phase can only develop locally, as the OA domains are too small to be observable by optical investigation, cannot be decided at present.

In summary, first benzil derivatives forming a series of LC phases, ranging from lamellar via two types of  $\text{Cub}_{\text{bi}}$  phases to columnar, have been obtained. Mirror symmetry breaking is observed in three of the soft matter phases, the isotropic liquid, the liquid crystalline  $\text{Cub}_{\text{bi}}/I23^{[*]}$  phase and in the soft crystalline phase ( $\text{Cr}_{\text{Iso}}^{[*]}$ ). This work contributes to the understanding of the development of mirror symmetry breaking in isotropic liquids as a consequence of network formation and increasing network-connectivity (Fig. 3e). In addition, these molecules with a bend around the central  $\text{O}=\text{C}-\text{C}=\text{O}$  bond appear to provide the still missing link between the mirror symmetry broken modes of soft self-assembly observed in polycatenars and in bent-core LC systems,<sup>6,15,16,33,36b,38</sup> bent mesogenic dimers<sup>6,16,36a</sup> and oligomers.<sup>39</sup> Moreover, as the  $\text{Iso}_1^{[*]}$  and  $\text{Cub}_{\text{bi}}/I23^{[*]}$  phases



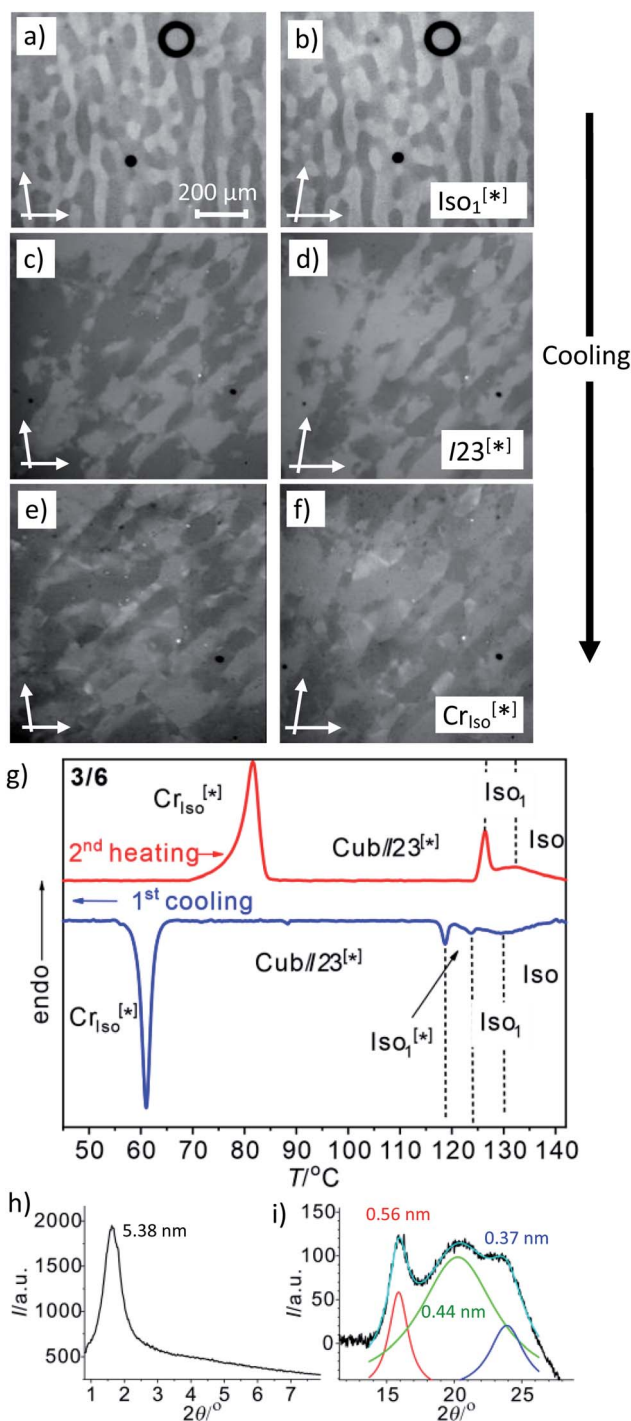


Fig. 4 The mirror symmetry broken mesophases of compound 3/6. (a–f) Conglomerates of optically active domains: (a and b) in the liquid  $\text{Iso}_1^{[*]}$  phase at 120 °C; (c and d) in the LC  $\text{Cub}_{bi}/23^{[*]}$  phase at 110 °C and (e and f) in the soft crystalline  $\text{Cr}_{\text{Iso}}^{[*]}$  phase at 60 °C, as observed on cooling between slightly uncrossed polarizers rotated by 5°; (a, c and e) in the anticlockwise and (b, d and f) in the clockwise direction (contrast enhanced). (g) DSC heating and cooling traces (10 K min<sup>-1</sup>); (h) small angle and (i) wide angle XRD pattern in the  $\text{Cr}_{\text{Iso}}^{[*]}$  phase at 50 °C (see also Fig. S12† for the complete diffraction pattern and Fig. S13† for the diffraction pattern of 3/10).

can provide giant chirality amplification,<sup>6,13</sup> the homogeneously chiral crystalline networks, once developed from these spontaneously mirror symmetry broken soft matter states, could be of interest as chiral templates for chiral recognition and separation, and the emerging field of dynamic enantioselective catalysis.<sup>37,39,40</sup>

## Conflicts of interest

There are no conflicts to declare.

## Acknowledgements

This work was supported by the Deutsche Forschungsgemeinschaft (Ts 39/24-2), the National Natural Science Foundation of China (No. 21761132033, 21774099 and 21374086) and the Science and Technology Agency of Shaanxi Province (2016KW-050 and 2018KWZ-03). The authors are grateful to Beamline BL16B1 at SSRF (Shanghai Synchrotron Radiation Facility, China) for providing the beamtime.

## References

- 1 A. Guijarro and M. Yus, *The Origin of Chirality in the Molecules of Life*, RSC, Publishing, Cambridge, 2009.
- 2 K. Soai, T. Kawasaki and A. Matsumoto, *Chem. Rec.*, 2014, **14**, 70–83.
- 3 D. B. Amabilino and R. M. Kellogg, *Isr. J. Chem.*, 2011, **51**, 1034–1040.
- 4 C. Viedma, *Phys. Rev. Lett.*, 2005, **94**, 065504; P. Cintas and C. Viedma, *Chirality*, 2012, **24**, 894–898; J. E. Hein, B. H. Cao, C. Viedma, R. M. Kellogg and D. G. Blackmond, *J. Am. Chem. Soc.*, 2012, **134**, 12629–12636.
- 5 R. R. E. Steendam, J. M. M. Verkade, T. J. B. van Benthem, H. Meekes, W. J. P. van Enkevort, J. Raap, F. P. J. T. Rutjes and E. Vlieg, *Nat. Commun.*, 2014, **5**, 5543; N. Uemura, K. Sano, A. Matsumoto, Y. Yoshida, T. Mino and M. Sakamoto, *Chem.-Asian J.*, 2019, **14**, 4150–4153.
- 6 (a) C. Tschierske, *Liq. Cryst.*, 2018, **45**, 2221–2252; (b) C. Tschierske and G. Ungar, *ChemPhysChem*, 2016, **17**, 9–26.
- 7 C. J. Brown and R. Sadanaga, *Acta Crystallogr.*, 1965, **18**, 158–164.
- 8 T. Kawasaki, Y. Harada, K. Suzuki, T. Tobita, N. Florini, G. Palyi and K. Soai, *Chem. Lett.*, 2008, **10**, 4085–4088.
- 9 Q. Shen and K. Hagen, *J. Phys. Chem.*, 1987, **91**, 1357–1360.
- 10 Z. Pawelka, A. Koll and T. Zeegers-Huyskens, *J. Mol. Struct.*, 2001, **597**, 57–66.
- 11 D. T. McLaughlin, T. P. Thao Nguyen, L. Mengnjo, C. Bian, Y. H. Leung, E. Goodfellow, P. Ramrup, S. Woo and L. A. Cuccia, *Cryst. Growth Des.*, 2014, **14**, 1067–1076.
- 12 (a) C. Dressel, F. Liu, M. Prehm, X. B. Zeng, G. Ungar and C. Tschierske, *Angew. Chem., Int. Ed.*, 2014, **126**, 13331–13336; (b) M. Alaasar, S. Poppe, Q. Dong, F. Liu and C. Tschierske, *Chem. Commun.*, 2016, **52**, 13869–13872.
- 13 (a) C. Dressel, T. Reppe, M. Prehm, M. Brautzsch and C. Tschierske, *Nat. Chem.*, 2014, **6**, 971–977; (b) C. Dressel, W. Weissflog and C. Tschierske, *Chem. Commun.*, 2015, **51**,

- 15850–15853; (c) M. Alaasar, M. Prehm, Y. Cao, F. Liu and C. Tschierske, *Angew. Chem., Int. Ed.*, 2016, **55**, 312–316; (d) M. Alaasar, S. Poppe, Q. Dong, F. Liu and C. Tschierske, *Angew. Chem., Int. Ed.*, 2017, **56**, 10801–10805.
- 14 D. R. Link, G. Natale, R. Shao, J. E. MacLennan, N. A. Clark, E. Korblova and D. M. Walba, *Science*, 1997, **278**, 1924–1927.
- 15 R. A. Reddy and C. Tschierske, *J. Mater. Chem.*, 2006, **16**, 907–961.
- 16 K. V. Le, H. Takezoe and F. Araoka, *Adv. Mater.*, 2017, 1602737.
- 17 *Bicontinuous Liquid Crystals*, ed. M. L. Lynch and P. T. Spicer, CRC Press, Taylor & Francis Group, Boca Raton, FL, 2005.
- 18 (a) S. Kutsumizu, *Isr. J. Chem.*, 2012, **52**, 844–853; (b) G. Ungar, F. Liu and X. B. Zeng, in *Handbook of Liquid Crystals*, ed. J. W. Goodby, P. J. Collings, T. Kato, C. Tschierske, H. F. Gleeson and P. Raynes, Wiley-VCH, 2nd edn, 2014, vol. 5, pp. 363–436.
- 19 Y. Yamamura, Y. Nakazawa, S. Kuzumizu and K. Saito, *Phys. Chem. Chem. Phys.*, 2019, **21**, 23705–23712.
- 20 H. T. Nguyen, C. Destrade and J. Malthete, *Adv. Mater.*, 1997, **9**, 375–388; D. W. Bruce, *Acc. Chem. Res.*, 2000, **33**, 831–840.
- 21 I. Nishiyama, *Chem. Rec.*, 2009, **9**, 340–355; M. Yoneya, *Chem. Rec.*, 2011, **11**, 66–76.
- 22 E. Nishikawa, J. Yamamoto and H. Yokoyama, *J. Mater. Chem.*, 2003, **13**, 1887–1893; E. Nishikawa and E. T. Samulski, *Liq. Cryst.*, 2000, **27**, 1463–1471; A. Yoshizawa, *Polym. J.*, 2012, **44**, 490–502; S. Kutsumizu, I. Tokiwa, A. Kawafuchi, Y. Miwa, Y. Yamamura and K. Saito, *Phys. Chem. Chem. Phys.*, 2016, **18**, 9013–9020.
- 23 A. M. Levelut and M. Clerc, *Liq. Cryst.*, 1998, **24**, 105–115.
- 24 X. B. Zeng, G. Ungar and M. Imperor-Clerc, *Nat. Mater.*, 2005, **4**, 562–567.
- 25 X. B. Zeng and G. Ungar, *J. Mater. Chem. C*, 2020, **8**, 5389–5398.
- 26 S. Debnath, H. F. Srouf, B. Donnio, M. Fourmigue and F. Camerel, *RSC Adv.*, 2012, **2**, 4453–4462.
- 27 X. B. Zeng, S. Poppe, A. Lehmann, M. Prehm, C. L. Chen, F. Liu, H. J. Lu, G. Ungar and C. Tschierske, *Angew. Chem., Int. Ed.*, 2019, **58**, 7375–7379.
- 28 This is in contrast to a previous series of rod-like molecules with only two terminal chains, forming a similar sequence  $Ia\bar{3}d-I23^{[*]}-Ia\bar{3}d$  with the growing chain length, but with an increasing  $d$ -value.<sup>18a,19</sup>
- 29 T. Reppe, C. Dressel, S. Poppe and C. Tschierske, *Chem. Commun.*, 2020, **56**, 711–713.
- 30 S. Kutsumizu, S. Miisako, Y. Miwa, M. Kitagawa, Y. Yamamura and K. Saito, *Phys. Chem. Chem. Phys.*, 2016, **18**, 17341–17344.
- 31 J. W. Goodby, D. A. Dunmur and P. J. Collings, *Liq. Cryst.*, 1995, **19**, 703–709.
- 32 H. R. Brand and H. Pleiner, *Eur. Phys. J. E*, 2017, **40**, 34.
- 33 (a) L. E. Hough, H. T. Jung, D. Krüerke, M. S. Heberling, M. Nakata, C. D. Jones, D. Chen, D. R. Link, J. Zasadzinski, G. Heppke, J. P. Rabe, W. Stocker, E. Korblova, D. M. Walba, M. A. Glaser and N. A. Clark, *Science*, 2009, **325**, 456–460; (b) L. E. Hough, M. Spannuth, M. Nakata, D. A. Coleman, C. D. Jones, G. Dantlgraber, C. Tschierske, J. Watanabe, E. Korblova, D. M. Walba, J. E. MacLennan, M. A. Glaser and N. A. Clark, *Science*, 2009, **325**, 452–456.
- 34 M. Alaasar, M. Prehm and C. Tschierske, *Chem.-Eur. J.*, 2016, **22**, 6583–6597; M. Alaasar, M. Prehm, M. Brautzsch and C. Tschierske, *J. Mater. Chem. C*, 2014, **2**, 5487–5501; M. Alaasar, M. Prehm, M. Brautzsch and C. Tschierske, *Soft Matter*, 2014, **10**, 7285–7296; M. Alaasar, M. Prehm and C. Tschierske, *Chem.-Eur. J.*, 2016, **22**, 6583–6597.
- 35 S. Shadpour, A. Nemati, N. J. Boyd, L. Li, M. E. Prevot, S. L. Wakerlin, J. P. Vanegas, M. Salamonczyk, E. Hegmann, C. Zhu, M. R. Wilson, A. I. Jakli and T. Hegmann, *Mater. Horiz.*, 2019, **6**, 959–968.
- 36 (a) A. Zep, M. Salamonczyk, N. Vaupotic, D. Pociecha and E. Gorecka, *Chem. Commun.*, 2013, **49**, 3119–3121; (b) J. Matraszek, N. Topnani, N. Vaupotic, H. Takezoe, J. Mieczkowski, D. Pociecha and E. Gorecka, *Angew. Chem., Int. Ed.*, 2016, **55**, 3468–3472.
- 37 Z. Shen, Y. Sang, T. Wang, J. Jiang, Y. Meng, Y. Jiang, K. Okuro, T. Aida and M. Liu, *Nat. Commun.*, 2019, **10**, 3976.
- 38 Cubic phases of bent core mesogens: R. A. Reddy, U. Baumeister, C. Keith, H. Hahn, H. Lang and C. Tschierske, *Soft Matter*, 2007, **3**, 558–570; S. Kang, M. Harada, X. Li, M. Tokita and J. Watanabe, *Soft Matter*, 2012, **8**, 1916–1922; J. Matraszek, J. Zapala, J. Mieczkowski, D. Pociecha and E. Gorecka, *Chem. Commun.*, 2015, **51**, 5048–5051.
- 39 A. Yoshizawa and M. Kurata, *New J. Chem.*, 2019, **43**, 8865–8868.
- 40 Y. Nagata, R. Takeda and M. Sugimoto, *ACS Cent. Sci.*, 2019, **5**, 1235; S. E. Denmark, *ACS Cent. Sci.*, 2019, **5**, 1117–1119.

